# CARDIAC MOTION AND MATERIAL PROPERTIES ANALYSIS USING DATA CONFIDENCE WEIGHTED EXTENDED KALMAN FILTER FRAMEWORK

*Huafeng Liu, Lung Ngong Wong, and Pengcheng Shi*

Biomedical Research Laboratory, Department of Electrical and Electronic Engineering
Hong Kong University of Science and Technology, Clear Water Bay, Hong Kong

## ABSTRACT

A biomechanical model constrained stochastic finite element framework has been developed to jointly estimate myocardium kinematics and material parameters from medical image sequence. In an extended Kalman filter formulation, we have observed that the augmented state error covariance matrix must be carefully chosen in order to avoid divergence. In this paper, we incorporate confidence measures of the input imaging and imaging-derived data into the initialization of the state error covariance matrix. These confidence measures come from the shape-matching process of boundary points and from the local phase coherence of the magnetic resonance velocity images. Experiments with two types of imaging inputs have shown vastly improved filtering efficiency and physiologically meaningful results.

## 1. INTRODUCTION

Myocardial ischemia can be identified and localized through the detection of kinematic and mechanics abnormalities of the left ventricle (LV) [1]. Efforts using optimal filtering strategies for recovering cardiac motion and deformation from medical image sequences have been reported [2, 3, 4]. Recently, we have proposed a stochastic finite element framework for simultaneous estimation of myocardial kinematics functions and material model parameters [5]. With the system dynamics equations of the heart, an extended Kalman filter (EKF) has been used to linearize the augmented equations and to provide joint estimation of kinematics and material parameters.

One key issue in EKF estimation arises from the fact that all filter parameters, e.g. the initial augmented state error covariance matrix and the process and measurement noise covariance matrices, have to be known exactly [6]. Incorrect selection of these parameters will result in large estimation errors or even divergence. In our actual implementation of the filter, the noise covariance is usually measured or estimated prior to the operation of the filter, while the determination of the initial augmented state error covariance is generally more difficult due to the complexity of the cardiac dynamics, the incomplete noisy imaging/imaging-derived data, and uncertainties of the constraining material model parameters. In this paper, we present a weighting technique for the initialization of the EKF state error covariance matrix that incorporates two confidence measures on imaging and imaging-derived data. We will show experimentally that this strategy speeds up the convergence of the estimation framework and provides more accurate and physiologically sensible results.

Thanks to Hong Kong Research Grant Council for CERG HKUST6057/00E, and to Hong Kong University of Science and Technology for a Postdoctoral Fellowship Matching Fund

## 2. BIOMECHANICALLY CONSTRAINED JOINT ESTIMATION FRAMEWORK

The finite element method (FEM) is a numerical analysis technique for obtaining approximate solutions to a wide variety of engineering problems, especially continuum mechanics ones [7]. The key to our analysis framework is that stochastic differential equations of LV dynamics are combined with FEM to study the myocardium dynamic behavior, including the uncertainties in their parameters and measurements. The Delaunay triangulated finite element mesh of the left ventricle is bounded by automatically segmented endocardium and epicardium (see Fig.2). Specifically, an isoparametric formulation defined in a natural coordinate system is used, in which the interpolation of the element coordinates and element displacements use the same basis functions. For linear isotropic material, the governing equations of the LV dynamics are expressed in matrix form:

$$M\ddot{U} + C\dot{U} + KU = R \tag{1}$$

where $U$ is the displacement vector, $R$ is the load vector, mass matrix $M$ is a function of myocardium density, and stiffness matrix $K$ is a function of the strain-stress matrix that is associated with two material specific parameters, the Young's modulus $E$ and the Poisson's ratio $\nu$. The damping matrix $C$ is constructed by assuming Rayleigh damping through $C = \alpha M + \beta K$.

The dynamics equations can then be re-written in state

space form [5]:

$$x(t+1) = A(\theta)x(t) + B(\theta)w(t) + v(t) \quad (2)$$
$$y(t) = Dx(t) + e(t) \quad (3)$$

where the material parameter vector $\theta$, the state vector $x$, the system matrices $A$ and $B$, and the control input $w$ are:

$$\theta = \begin{bmatrix} E \\ \nu \end{bmatrix}, \quad x(t) = \begin{bmatrix} U(t) \\ \dot{U}(t) \end{bmatrix}, \quad w(t) = \begin{bmatrix} 0 \\ R \end{bmatrix}$$
$$A = e^{A_c T}, \quad B = A_c^{-1}(e^{A_c T} - I)B_c$$
$$A_c = \begin{bmatrix} 0 & I \\ -M^{-1}K & -M^{-1}C \end{bmatrix}$$
$$B_c = \begin{bmatrix} 0 & 0 \\ 0 & M^{-1} \end{bmatrix}$$

$v(t)$ and $e(t)$ are the process and measurement noises which are white and zero mean ($E[v(t)] = 0, E[v(t)v(s)'] = Q_v(t)\delta_{ts}, E[e(t)] = 0, E[e(t)e(s)'] = R_e(t)\delta_{ts}$), $y(t)$ is the imaging/imaging-derived data, $D$ is a known measurement matrix, and $T$ is the temporal sampling interval. The unknown parameter vector $\theta$ is treated as a part of an augmented state vector, and the augmentation leads to a solution of the nonlinear filtering based on extended Kalman filter:

$$\hat{x}(t+1) = A(\hat{\theta}(t))\hat{x}(t) + B(\hat{\theta}(t))w(t) + L(t)\left[y(t) - D\hat{x}(t)\right] \quad (4)$$
$$\hat{\theta}(t+1) = \hat{\theta}(t) + G(t)\left[y(t) - D\hat{x}(t)\right] \quad (5)$$

where

$$L(t) = \left[A(\hat{\theta}(t))P_1(t)D^T + M_t P_2^T(t)D^T\right]S^{-1}(t)$$
$$G(t) = P_2^T(t)D^T S^{-1}(t)$$
$$P_1(t+1) = A(\hat{\theta}(t))\left[P_1(t)A^T(\hat{\theta}(t)) + P_2(t)M_t^T\right] + M_t\left[P_2^T(t)A^T(\hat{\theta}(t)) + P_3(t)M_t^T\right] + Q_v - L(t)S(t)L^T(t)$$
$$P_2(t+1) = A(\hat{\theta}(t))P_2(t) + M_t P_3(t) - L(t)S(t)G^T(t)$$
$$P_3(t+1) = P_3(t) - G(t)S(t)G^T(t)$$
$$S(t) = DP_1(t)D^T + R_e$$
$$M_t = \frac{\partial}{\partial\theta}(A(\theta)\hat{x} + Bw(t))\Big|_{\theta=\hat{\theta}}$$

with initial conditions:

$$P(0) = \begin{bmatrix} P_1(0) & P_2(0) \\ P_2^T(0) & P_3(0) \end{bmatrix}$$
$$\hat{x}(0) = \hat{x}_0, \quad \hat{\theta}(0) = \hat{\theta}_0$$

In our earlier implementation [5], the augmented state error covariance sub-matrices $P_1(0)$ (state), $P_2(0)$ (state-material correlation), and $P_3(0)$ (material) are modeled as diagonal matrices. $P_1(0)$ has separate uniform values for displacement data and velocity data. The motivation to construct non-uniform $P_1(0)$ sub-matrix comes from the observation that the filter performance is very sensitive to the initial values. Because of the periodic nature of the cardiac dynamics, we cyclically feed the updated imaging and imaging-derived data into the filtering framework until reaching convergence. Causal and improper selections of the initial values often *destroy* the integrity of the finite element mesh during the filtering process. Further, we believe that any prior or educated knowledge of the state and material parameters should enable us to achieve higher filtering efficiency and more robust results.

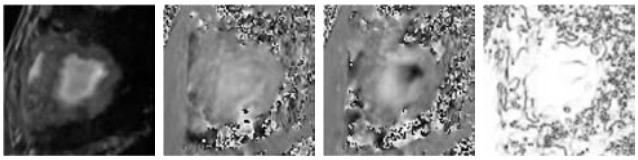

intensity x-velocity y-velocity LPC value

**Fig. 1**. Canine cardiac MR phase contrast images.

## 3. DATA CONFIDENCE WEIGHTING

The state error covariance sub-matrix $P_1(0)$ can be expressed as $P_1(0) = diag(P_{UU}(0), P_{\dot{U}\dot{U}}(0))$ . The first term on the diagonal is the variance of the displacements, and in our current implementation it is related to confidence measures of the shape-matched boundary point displacements. The second term, the variance of the velocity, is related to the confidence measures of the phase contrast velocity information of MR imaging that are characterized by the local phase coherence values [8]. The initial values of $P_2(0)$ sub-matrix are set to zeroes. And $P_3(0)$ is the covariance sub-matrix of material parameters $E$ and $\nu$, whose values are proportional to the expected errors in the corresponding parameter to ensure smooth convergence.

### 3.1. Confidence measures on shape-matched boundary displacements

We had previously proposed a strategy for myocardial boundary motion tracking based on locating and matching differential geometric landmarks [9]. Based on the hypothesis the LV boundary contours deform as little as possible between successive temporal frames, bending energy measure is used as the matching criterion to obtain the point correspondences between contours:

$$\min_{\varphi\in\mathcal{C}} e_{bend}(\phi,\varphi) = \min_{\varphi\in\mathcal{C}}[\kappa_f(\phi) - \kappa_s(\varphi)]^2 \quad (6)$$

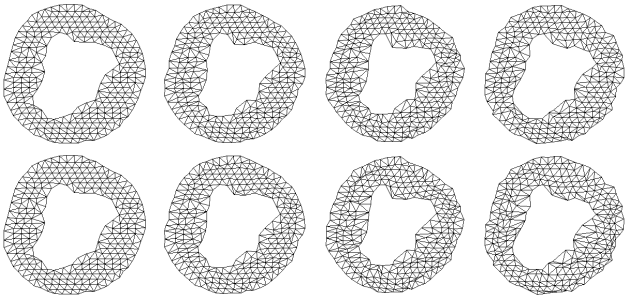


**Fig. 2**. Deforming finite element mesh of the left ventricle: using boundary displacements (first row), and using boundary displacements and mid-wall velocity (second row).

where $\kappa_f(\phi)$ is the curvature for a point $\phi$ in the first contour, $\mathcal{C}$ the corresponding search region on the second contour, and $\kappa_s(\varphi)$ the curvature of a candidate point $\varphi$ within the search region. Among all the candidate points, the one at $\xi$ which yields the smallest bending energy is chosen as the matched point, and the bending energy value indicates the goodness $m_g(\xi) = e_{bend}(\phi, \xi)$ of the match.

Further, the bending energy measures for all other points within the search region are also recorded as the basis to measure the uniqueness of the matching choice. Ideally, the bending energy value of the chosen point should be an outlier (much smaller value) compared to the values of the rest of the candidate points. If we denote the mean value of the bending energy measures of all the points inside the search window except the chosen point as $\bar{e}_{bend}$ and the standard deviation as $\sigma_{bend}$, we define the uniqueness measure of the match as:

$$m_u(\xi) = |\frac{e_{bend}(\phi, \xi)}{\bar{e}_{bend} - \sigma_{bend}}| \tag{7}$$

Obviously for both goodness and unique measures, the smaller the values the more reliable the match. Combining these two together, we arrive at a *confidence measure* for the matched second contour point $\xi$ of the first contour point $\phi$:

$$c(\xi) = \frac{1}{k_{1,g} + k_{2,g} m_g(\xi)} \frac{1}{k_{1,u} + k_{2,u} m_u(\xi)} \tag{8}$$

where $k_{1,g}, k_{2,g}, k_{1,u}$, and $k_{2,u}$ are normalizing constants such that the confidence measures for all point matches between contours are in the range of 0 to 1.

This process yields a set of shape-based, best-matched displacement vectors for each pair of contours, and each vector has an associated confidence measure. Elements of the displacement error sub-matrix $P_{UU}(0)$ will be weighted by $(1 - c(\xi))$.

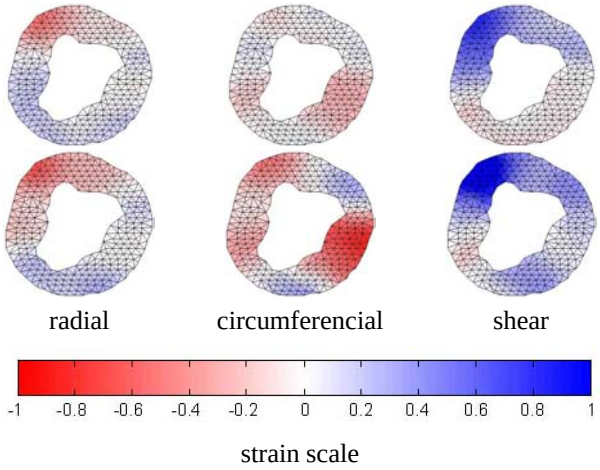


**Fig. 3**. Strain estimates between end-diastole and end-systole: using boundary displacements (first row), and using boundary displacements and mid-wall velocity (second row).

### 3.2. Confidence measures on mid-wall MR phase contrast velocity

Velocity and intensity images are acquired using the phase contrast cine magnetic resonance imaging. This imaging technique relies on the fact that a uniform motion of tissue in the presence of a magnetic field gradient produces a change in the MR signal phase that is proportional to velocity [10]. In principle, the instantaneous Euclidian velocities for the moving tissue can be easily obtained for each pixel in an image acquisition. However, because of the relatively large size of the imaging region-of-interest, current phase contrast velocity estimates near the endocardial and epicardial boundaries are extremely noisy, and reliable motion information is only available within the mid-wall region.

Local phase coherence (LPC) [8] is used to assess the reliability of the velocity data at mid-wall. For velocity vector $v_s$ at $s$ and velocity vector $v_i$ of its neighbor at $i$, we define the $LPC(v_s)$ to be:

$$f(v_s, v_i) = < v_s, v_i > / ||v_s|| \; ||v_i|| \tag{9}$$

$$LPC(v_s) = \frac{1}{16} \left[ \sum_{i=1}^{8} f(v_s, v_i) + 8 \right] \tag{10}$$

where the summation is taken over the eight neighbors. Since $f(v_s, v_i)$ is within $[-1, 1]$, the LPC value is thus within the range of $[0, 1]$.

In ideal situation, we should expect high LPC values at the velocity coherent regions of mid-wall myocardium. Any deviation from high LPC indicates poor quality of the velocity information. Elements of the velocity error sub-matrix $P_{\dot{U}\dot{U}}(0)$ now will be weighted by $(1 - LPC(v_s))$.

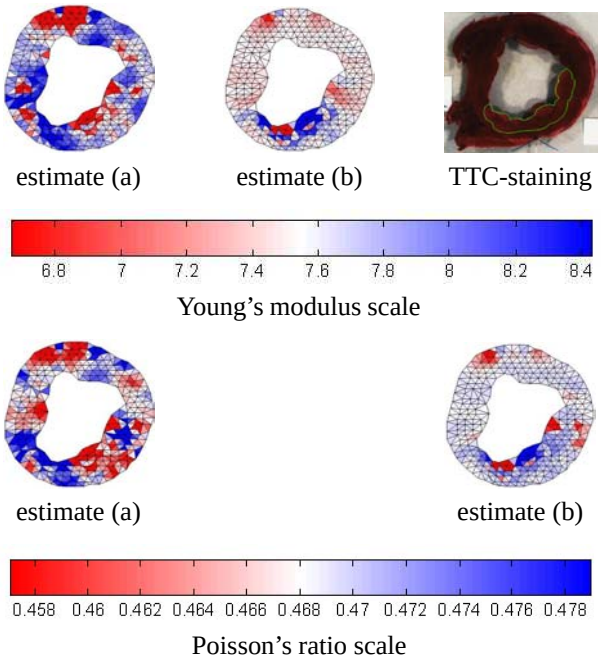


**Fig. 4**. Estimated material parameters and the TTC-stained post mortem myocardium. Young's modulus (first row): using boundary displacements (a), and using boundary displacements and mid-wall velocity (b). Poisson's ratio (second row): using boundary displacements (a), and using boundary displacements and mid-wall velocity (b).

## 4. EXPERIMENTS

Sixteen sets of MR velocity and magnitude images are acquired over the heart cycle [5]. Fig.1 shows the MR images and LPC map at end-diastole (ED). Myocardial boundaries are extracted using velocity constrained level set strategy, and boundary displacements between consecutive frames are detected based on locating and matching geometric landmarks and a local coherent smoothness model [9]. The LV is modeled as an isotropic linear elastic material, and represented by linear finite element mesh constructed from the Delaunay triangulation of the sampled points. Initial material parameters for the myocardium are set to 75,000 Pascal for Young's modulus and 0.47 for Poisson's ratio, and the myocardium mass density is set to 1.5 $gram/mm^3$. A data confidence measure weighted extended Kalman filter is employed to estimate tissue deformation and material parameters, by 1). using the shape-matched boundary displacements only, and 2). using both the mid-wall phase contrast velocity and boundary displacements.

Fig. 2 shows examples of the recovered LV mesh at multiple time frames. Fig. 3 shows the cardiac specific radial, circumferential, and shear strain distributions between ED and end-systole (ES). The final converged estimates of Young's modulus and Poisson's ratio are shown in Fig.4, along with picture of the gold-standard TTC-stained post mortem myocardium. Please note that while using both displacements and velocity data, there is very good agreement between our estimated infarcted tissues (stiffer Young's modulus and close to incompressible Poisson's ratio) and the highlighted histological results from TTC-staining.

## 5. CONCLUSIONS

To improve the filter performance, confidence measures of the imaging/imaging-derived measurement data are used in constructing the augmented state error covariance matrix. This data confidence measure weighted extended Kalman filter framework adopts temporal periodic characteristics of the heart motion as well as the mechanical modeling of the myocardium to estimate the kinematics and material parameters simultaneously. Initial experiments with real imaging data have been performed, and the results are in high agreement with the histological results of the same animal.

## 6. REFERENCES

[1] L. Glass, P. Hunter, and A. McCulloch, *Theory of Heart*, Springer-Verlag, New York, 1991.

[2] H. Liu and P. Shi, "Biomechanically constrained multiframe estimation of nonrigid cardiac kinematics from medical image sequence," in *International Conference on Inverse Problems and Numerics*, in press, 2002.

[3] J.C. McEachen, A. Nehorai, and J.S. Duncan, "Multiframe temporal estimation of cardiac nonrigid motion," *IEEE Trans. Image Proc.*, vol. 9, pp. 651–665, 2000.

[4] F.G. Meyer, R.T. Constable, A.J. Sinusas, and J.S. Duncan, "Tracking myocardial deformation using spatially constrained velocities," *IEEE Trans. Med. Imag.*, vol. 15, no. 4, pp. 453–465, 1996.

[5] P. Shi and H. Liu, "Stochastic finite element framework for cardiac kinematics function and material property analysis," in *MICCAI*, 2002, pp. 634–641.

[6] A. Gelb, *Applied Optimal Control*, MIT Press, London, 1974.

[7] K.H. Huebner and E.A. Thornton, *The Finite Element Method for Engineers*, John Wiley & Sons, New York, 1982.

[8] A.C.S. Chung, J.A. Noble, and P. Summers, "Fusing speed and phase information for vascular segmentation of phase contrast MR angiograms," *Medical Image Analysis*, vol. 6, pp. 109–128, 2002.

[9] P. Shi, A. Sinusas, R.T. Constable, E. Ritman, and J. Duncan, "Point-tracked quantitative analysis of left ventricular motion from 3D image sequences," *IEEE Trans. Med. Imag.*, vol. 19, no. 1, pp. 36–50, 2000.

[10] N.J. Pelc, R.J. Herfkens, A. Shimakawa, and D. Enzmann, "Phase contrast cine magnetic resonance imaging," *Magnetic Resonance Quarterly*, vol. 7, no. 4, pp. 229–254, 1991.